ACS OMEGA

http://pubs.acs.org/journal/acsodf

Article

DFT Studies on a Metal Oxide@Graphene-Decorated D−π_1−π_2−A Novel Multi-Junction Light-Harvesting System for Efficient Dye-Sensitized Solar Cell Applications

Kaniz Fatima, Altaf Hussain Pandith,* Taniya Manzoor, and Aaliya Qureashi

Cite This: *ACS Omega* 2023, 8, 8865−8875

Read Online

ACCESS | Metrics & More | Article Recommendations | Supporting Information

ABSTRACT: Graphene nanocomposites have emerged as potential photoanode materials for increased performance of the dye-sensitized solar cells (DSSCs) via charge transfer. Various metal-oxide-decorated graphene nanocomposites have widespread applications in energy devices, such as solar cells, fuel cells, batteries, sensors, electrocatalysis, and photocatalysis. However, the possible role of these composites in DSSC applications has largely remained unexplored. Herein, we studied a Sb_2O_3-decorated graphene−D−π_1−π_2−A sensitized TiO_2 nanocomposite (dye-$(TiO_2)_9$/Sb_2O_3@GO) as a model multi-junction light-harvesting system and examined the impact of various π-bridges on the optical and photovoltaic properties of the push−pull dye system employed in this light-harvesting system. We have shown that by changing the spacer unit, the light sensitivity of nanocomposites can be varied from visible to near-infrared wavelengths. Furthermore, with the integration of metal-oxide-decorated graphene nanocomposites on D−π_1−π_2−A systems and D−π−A systems, composite photoelectrodes displayed better optical and photovoltaic characteristics with an enhanced absorption spectrum in the wavelength range of 800−1000 nm. The performance of the D−π_1−π_2−A system has been evaluated in terms of various photovoltaic parameters such as the highest occupied molecular orbital−lowest unoccupied molecular orbital energy gaps, excited-state oxidation potential (E^*_{dye}), free energy of electron injection (G_{inject}), total reorganization energy (λ_{total}), and open-circuit voltage (V_{oc}). This work throws light on the current trends and the future opportunities in graphene−metal oxide nanocomposite-based DSSCs for better harvesting of the solar spectrum and better performance of solar devices.

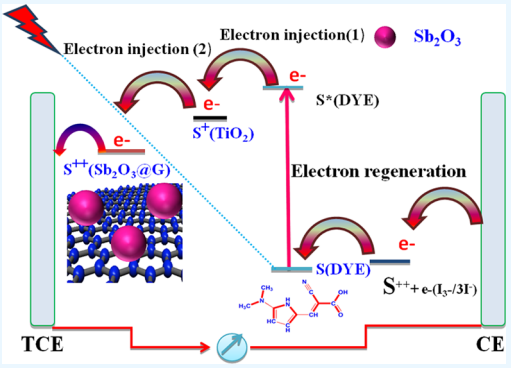

1. INTRODUCTION

Over the last few decades, the widespread use of fossil fuels has resulted in significant environmental contamination.[1−3] With the growing awareness of environmental preservation, sunlight is assuming tremendous importance as an alternate sustainable renewable energy source in a range of industries, including the agriculture sector and transportation, involving photovoltaic conversion technology.[4−7] Because of their easy production technique, low cost, and readily programmable optical aspect, the dye-sensitized solar cells (DSSCs) hold potential for a range of energy utilization applications. The DSSC was first discovered by O′Regan and Grätzel in 1988 during the search for a better-performance electrode.[8] The DSSC mainly consists of five main components such as a semiconductor, a transparent conducting electrode, a photosensitizer, an electrolyte, and a counter electrode. The photosensitizer, which is responsible for light harvesting, electron transfer, and injection, is regarded as a critical component among all the components. As a result, scientists are motivated to create and synthesize a wide variety of useful organic dyes, characterized by the type of raw materials used, the cost of materials involved, the flexibility of molecular design, enhanced light-harvesting efficiency (LHE), and fast electron transfer kinetics. Most of the metal-free organic dye photosensitizers comprise D−π−A units. Even minor alterations in the D−π−A system can modify the dye's whole electrochemical and photophysical characteristics.[9−11] Hence, the nature of the D−π−A system, in terms of molar absorptivity, electron transport, push−pull effects, and chemical stability, is the key factor on which the molecular sensitizer depends for acquiring more efficient solar cells. A strong and characteristic absorption band that can encompass the whole visible and infrared (IR) spectrum is necessary to improve the efficiency of DSSCs.[12−14] A variety of donor groups have been exploited such as quinoxaline, carbazole, porphyrin, and dimethylamine groups.[15−17] The π-spacer or the π-bridge attachment, due to its conjugation properties, leads to a shift of the absorption to the near-IR (NIR) region

Received: January 17, 2023
Accepted: February 7, 2023
Published: February 23, 2023

that will ultimately increase the open-circuit voltage (V_{oc}) values. The anchoring groups such as the cyano-acrylic acid and the carboxylic acid facilitate the electron injection processes due to their strong binding ability on metal oxide semiconductor nanoparticles such as TiO_2, besides making a molecular connection with the nanocomposite semiconductor surface.

Graphene is a carbon allotrope that consists of a honeycomb-like crystal lattice of tightly packed thin layers of sp^2 hybridized carbon atoms. It is recognized for its amazing capabilities and has sparked a lot of interest in material science, biology, chemistry, and physics.[18] As it consists of a theoretical surface area of 2630 $m^2\ g^{-1}$ and a carrier density of 1012 cm^{-2} at room temperature, it has the highest electrical conductivity of 106 S cm^{-1} and an excellent thermal conductivity (~5000 W $m^{-1}\ k^{-1}$).[19] It was first exploited mechanically by Geim and Novoselov in 2004 from graphite, for which they shared a Nobel prize in physics in 2010.[20] Because pristine graphene has been claimed to have no band gap, its capabilities in photosensitization processes have not been fully studied. However, by inserting oxygen-containing functional groups (−COOH, OH, and epoxides), graphene can be proposed as a promising alternative that may open up the zero band gaps and can be exploited for better practical application in optoelectronic industries.[21] After the decoration with various inorganic metal oxide nanoparticles, the light-stimulated electronic conduction of graphene can be enhanced and can be successfully employed in energy conversion devices and energy depots .[22]

Nanomaterials are widely known for their prospective applications in the fields of electronics, optoelectronics, thermoelectronics, and magnetism. In particular, antimony(III) oxide (Sb_2O_3) semiconductor nanostructures have attracted attention due to their potential use as flame retardants, UV filters, and optical devices. Sb_2O_3 nanostructures in the forms of nanoparticles, nanowires, nanoribbons, nanosheets, nanorods, and nanocrystals have been synthesized by several researchers.[23−27] Applications in optics, electronics, and optoelectronics benefit from the semiconducting properties of V and VI compounds. Sb_2O_3 is unique and intriguing because of its significant indirect band gap and band gap location close to the UV area.[28] Additionally, it works well as a UV filter for interferometric applications, UV light-emitting device (LED) technology, and solar cell technology.[29] Because of their high refractive index and strong abrasion resistance, Sb_2O_3 nanoparticles are also regarded as one of the key optical materials. Metal oxide decorated with graphene nanocomposites are extremely popular in the field of electrochemical energy storage.[30] They are used as electrode materials for electrical energy storage devices because of their favorable physicochemical properties, which include high thermal and chemical stability, excellent electrical conductivity, a large surface area, and superior thermal and mechanical capabilities.[31] Further, their wide potential range and varied surface chemistry have made it possible to personalize the characteristics of storage devices. It was fascinating to observe how mixing various polarized antimony and oxygen surfaces produced efficient electron/hole doping in graphene while preserving its exceptional electrical properties, thereby efficiently enhancing the visible/IR light absorption.

Numerous efforts have been made in the direction of developing an effective sensitizer. Finding a sensitizer that can effectively absorb photons over the whole solar spectrum has proven to be challenging. Therefore, innovative dye sensitizers need to be explored that exhibit superior absorption behavior and effective energy transfer. However, it is challenging for a single dye molecule to exhibit such a prolonged absorption behavior. In this regard, co-sensitization of semiconductor surfaces employing a variety of junctions can help in providing a broader and more intense absorption, which will improve the performance of the DSSCs. Sánchez-de-Armas et al.[32] examined the influence of TiO_2's computational size on anatase structures and reported that $(TiO_2)_9$ is big enough to mimic the actual electrical characteristics of anatase structures. Therefore, in this work, we have modeled the system by using the $(TiO_2)_9$[32,33] cluster size for the simulation of the optoelectronic properties of dye-sensitized TiO_2 nanoparticles. All the optoelectronic and photovoltaic parameters-related calculations on an isolated dye/TiO_2 system were performed using the GAUSSIAN 09 program employing localized basis sets. We co-sensitized a $D-\pi_1-\pi_2-A-(TiO_2)_9$ system (dimethylamine as a donor, pyrrole/furan/thiophene as a π-spacer, and cyano-acrylic acid as an acceptor) with Sb_2O_3-decorated graphene (Sb_2O_3@Graphene) as a multi-junction system (Figure 1). The effect of such co-sensitization on the

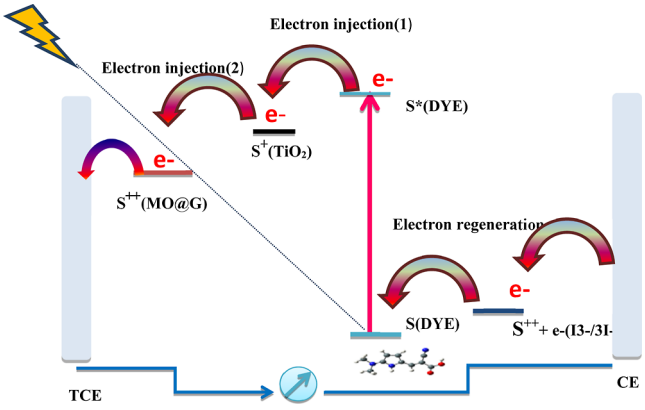

Figure 1. Schematic diagram of the DSSC.

absorption behavior and optoelectronic and photovoltaic properties of the TiO_2 systems was studied using density functional theory (DFT). We evaluated the performance of these photosensitized systems in terms of various parameters such as the highest occupied molecular orbital (HOMO), lowest unoccupied molecular orbital (LUMO), HOMO−LUMO energy gap, LHE, Φ_{INJ}, V_{oc}, ΔG_{reorg}, and ΔG_{inj}.

2. THEORETICAL BACKGROUND

2.1. Photoconversion Efficiency. To compute the performance of the solar cell, the most frequently used parameter for converting sunlight into electricity is its photoconversion efficiency (PCE).[34]

The PCE can be determined as shown in eq 1

$$\eta = J_{sc} V_{oc} FF / P_{inc} \quad (1)$$

From eq 1, V_{oc} is the open-circuit voltage, FF is the fill factor; J_{sc} is the short-circuit current density, and P_{inc} is the incident photon to current efficiency.

2.2. V_{oc} (Open-Circuit Voltage). V_{oc} is considered to be an important parameter, and it depends on various factors like charge carrier recombination, light sources, and the energy level of materials as shown in eq 2.

https://doi.org/10.1021/acsomega.3c00333
ACS Omega 2023, 8, 8865−8875

$$V_{oc} = E_{LUMO} - E_{CB} \quad (2)$$

Therefore, from eq 2, V_{oc} can be calculated by determining the energy difference between the LUMO of the dye and the conduction band (CB) of TiO_2.[35]

2.3. Light-Harvesting Efficiency. The LHE can be calculated according to eq 3

$$LHE = 1 - 10^{-f} \quad (3)$$

From eq 3, the higher the oscillator strength is, the higher the LHE will be. Therefore, the LHE is an important factor to explore the role of the dye in a DSSC.[36]

2.4. ΔG_{inj} (Electron Injection Ability). The free energy changes for injecting an electron from the dye-excited state to the CB is known as the electron injection ability (ΔG_{inj}). The energy level differences between the dye's excited-state LUMO level and the semiconductor TiO_2 E_{CB} is the driving factor for electron injection from a dye to a semiconductor TiO_2. The negative sign of ΔG_{inj} denotes the process's spontaneity.

It is suggested that the higher the ΔG_{inj} values are, the higher the Φ_{inject} values will be.[37] Therefore, ΔG_{inj} can be calculated as per eq 4

$$\Delta G_{inj} = E_{ox}^{dye*} - E_{CB} \quad (4)$$

From eq 4, E_{ox}^{dye*} is the excited state of the oxidation potential energy and can be calculated as shown in eq 5.[38]

$$E_{ox}^{dye*} = E_{ox}^{dye} - \lambda_{max}^{ICT} \quad (5)$$

From eq 5, *E*oxdye is the ground-state reduction potential, which is equal to $-E_{HOMO}$.[39] λ_{max}^{ICT} is the transition energy corresponding to λ_{max}.

2.5. ΔG_{reg} (Electron Regeneration). From eq 6,ΔG_{reg} is another parameter that influences the efficiency of the DSSC. To acquire the fastest electron transfer process, it is necessary to have lower regeneration values according to eq 6.[40]

$$\Delta G_{reg} = E_{ox}^{dye} - E_{redox} \quad (6)$$

where E_{redox} is the redox potential of electrolytes.

2.6. ΔG_{reorg} (Reorganization Energy). The pace of intramolecular electron transfer, according to the Marcus model,[41] is primarily determined by the reorganization energy. When transitioning from a neutral geometry to a charged state geometry and vice versa, the structural relaxation of the oxidized or reduced state geometries along internuclear coordinates causes total intramolecular reorganization for electron transfer. As a result, a lower λ_{total} value suggests a faster charge transport carrier across the intermolecular interface. As a result, we calculated the reorganization energy of holes and electrons using the following relationships[42]

$$\Lambda_{e/h} = \lambda_1 + \lambda_2$$

where, from eqs 7 and 8, $\lambda_{e/h}$ is calculated as single-point energy differences between the anion/cation at a neutral molecule and the anion/cation at the optimized geometry

$$\lambda_1 = E^{+/-}(G^0) - E^{+/-}(G^{+/-}) \quad (7)$$

$$\lambda_2 = E^0(G^{+/-}) - E^0(G^0) \quad (8)$$

3. Computational Details. DFT and time-dependent DFT (TD-DFT) simulations were used to explore the photovoltaic characteristics of six D−π−A (DA1) and D−π_1−π_2−A (DA2−DA6) dye systems, where dimethyl as the donor, pyrole/furan/thiophene/as the spacer unit, and cyanoacrylic acid as an anchoring group were used, using the Gaussian 09 set of codes.[43] The DFT technique paired with the B3LYP exchange−correlation functional and the 6-311G(d,p) basis set was used to optimize the geometry of all compounds in the ground state.[44] B3LYP is a suitable harmonic function for investigating the value properties of tiny and large organic π−π* conjugated compounds.[45] We employed the B3LYP method to compute the excitation energies and the solvent effects [tetrahydrofuran (THF)] on the absorption spectra. DFT, at the B3LYP/6-311G[46−48] level of theory, was used to optimize the geometry of all dyes. This level of theory has been reported to yield accurate results for the similar type of systems.[49−52] The optimum structures were confirmed to be actual local minima (without imaginary frequency) on the potential energy surface using frequency analysis. At the B3LYP/6-311G(d,p) level of theory, molecular orbitals such as the HOMO and LUMO were calculated. The solvent calculation was carried out in THF using a conductor-like polarizable continuum model (CPCM).[53] The same method was used to calculate photovoltaic characteristics. TD-DFT appears to be effective in estimating optical absorption, electronic characteristics, and vertical excitation energy. TD-DFT is also thought to have optimum accuracy in the case of extended conjugated systems and charge transfer excitations.[54] The total density of states (TDOS) data were calculated using Gauss Sum software.[55]

4. RESULTS AND DISCUSSION

4.1. Optimization and Molecular Geometries. We designed a D−π−A system, where in dimethylamine acts as a donor, pyrrole acts as a π-bridge, and cyanoacrylic acid acts as an anchoring group, and this dye system was optimized and named DA1 (Figure 2a). Subsequently, another π-bridge was incorporated next to the previously attached π-bridge and named DA2, DA3, and DA4, respectively, for pyrrole, furan, and thiophene being used as the second π-bridge (Figure 2b−d). Furthermore, in order to compare the photovoltaic and optoelectronic properties, we optimized two systems with a π-bridging system consisting of furan−furan and thiophene−thiophene groups (DA5 and DA6, respectively) as shown in Figure 2e,f. The DFT technique paired with the B3LYP exchange−correlation functional and 6-311G(d,p) basis set

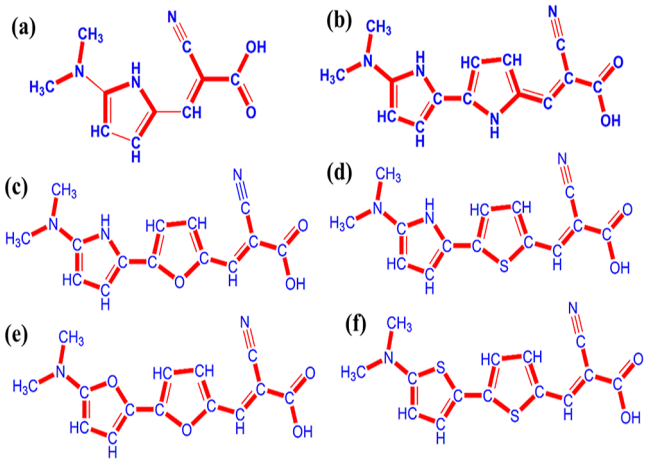

Figure 2. (a−f) Chemical structure of DA1−DA6 molecules.

https://doi.org/10.1021/acsomega.3c00333
ACS Omega 2023, 8, 8865−8875

Table 1. Optoelectronic Properties of DA1−DA6 Systems

	dye			dye−$(TiO_2)_9$			dye−$(TiO_2)_9$−MO@G		
mol	E_{LUMO} (eV)	E_{HOMO} (eV)	E_{GAP} (eV)	E_{LUMO} (eV)	E_{HOMO} (eV)	E_{GAP} (eV)	E_{LUMO} (eV)	E_{HOMO} (eV)	E_{GAP} (eV)
DA1	−2.28	−5.89	3.61	−3.38	−5.59	2.21	−2.82	−4.39	1.57
DA2	−2.45	−4.93	2.48	−3.28	−5.16	1.88	−2.72	−4.36	1.64
DA3	−2.75	−5.15	2.40	−3.397	−5.35	1.95	−2.94	−4.37	1.43
DA4	−2.59	−4.88	2.29	−3.44	−5.07	1.63	−2.82	−4.38	1.56
DA5	−2.92	−5.21	2.29	−3.53	−5.56	2.03	−3.13	−4.38	1.25
DA6	−2.68	−5.36	2.68	−3.58	−5.34	1.76	2.96	−4.39	1.43

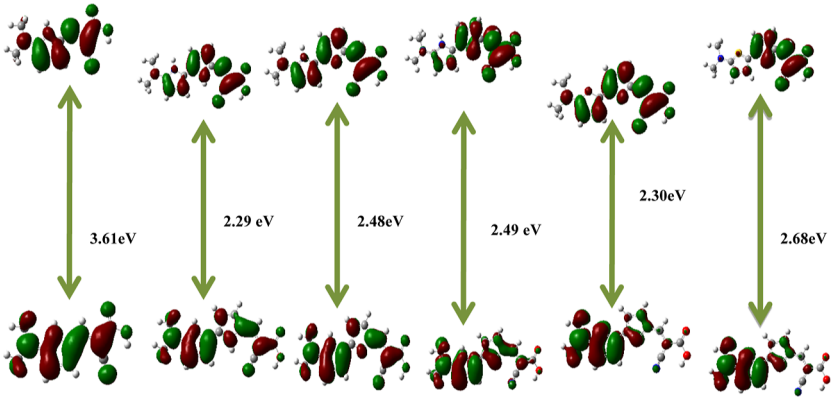

Figure 3. HOMO−LUMO energy gaps of various dyes of systems DA1−DA6.

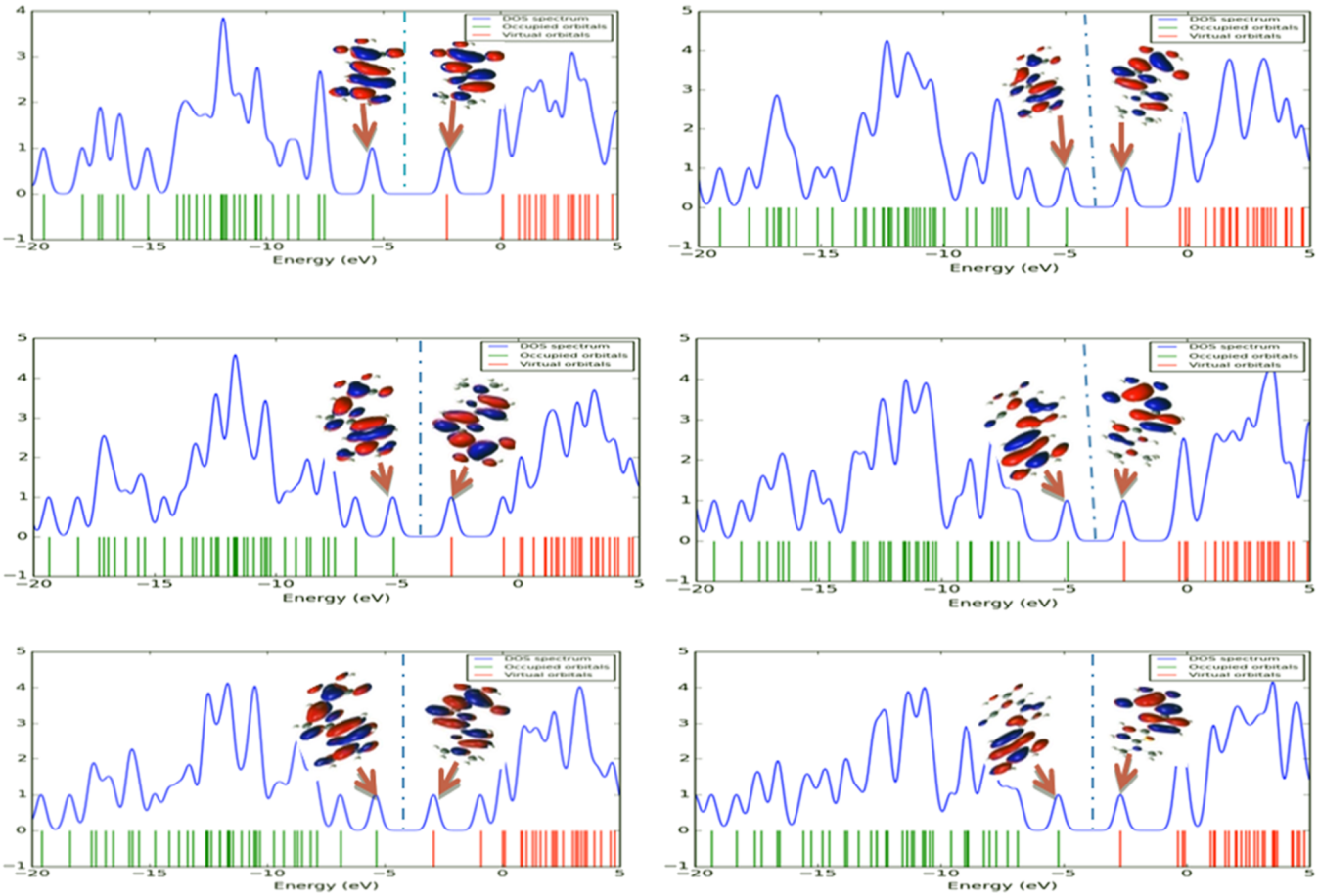

Figure 4. TDOS of DA1−DA6 systems.

was used to optimize the geometry of all the dye molecules (DA1−DA6). This was followed by anchoring these optimized dyes on TiO_2 systems. Finally, we studied the interactions of dye−$(TiO_2)_9$ systems with Sb_2O_3@graphene for modeling a

https://doi.org/10.1021/acsomega.3c00333
ACS Omega 2023, 8, 8865−8875

multi-junction system to expand the absorption spectrum. The effect of such an interaction on the overall photovoltaic properties was studied. The novelty of this study is that it involves the co-sensitization of TiO_2 with Sb_2O_3@graphene and dye sensitizers and then examining the relationship between the interface structure and properties in order to build a fundamental physical picture of a nanocomposite. Excited-state electron transfer parameters were also computed to understand the composite's charge transport properties. In this study, dimethylamine is used as a donor (D),[56−61] pyrrole/furan/thiophene, are used as π bridges, and cyanoacrylic acid is used as an anchoring group.[62−71]

4.2. Electronic Structure. The HOMO, LUMO, and HOMO−LUMO gaps were obtained for all six systems (DA1−DA6) in Table1. It was found that the HOMO values for all the systems were as follows: −5.89, −4.93, −5.15, −4.88, 5.21, and −5.36 eV for DA1, DA2, DA3, DA4, DA5, and DA6, respectively. Moreover, the LUMO energies were −2.28, 2.45, 2.75, 2.59, 2.92, and 2.68 eV for DA1, DA2, DA3, DA4, DA5, and DA6, respectively. For thermodynamic feasibility of electron transfer from the excited state of the dye to the semiconductor CB, the band edges of the oxidation states of the dye and reduction states of the semiconductor CB must overlap and the dye LUMO energy level must lie higher than the semiconductor CB for effective electron injection while the HOMO energy level of dye must lie lower than the redox potential of the electrolyte. From our calculations, it is evident that for all the systems, LUMO energy levels are situated above the TiO_2 CB edge position of dye−TiO_2−MO@G, while its HOMO levels are situated below the redox potential of the redox mediator. It was also found that the energy gap of all the systems lie in the range of 2.29−3.61 eV. The schematic diagram of the molecular orbital energy of the DA1−DA6 systems is shown in Figure 3. From the diagram, it is clear that the LUMO energies of all the model systems are more than the energy of the TiO_2 CB, showing the directionality of electron transfer, whereas the HOMO energies of all the dyes are lower than the redox potential of the redox mediator, which is necessary for efficient charge regeneration.

To support these generalizations, the TDOS has been calculated for all the DA1−DA6 systems, using the B3LYP/6-311G(d,p) level of theory, in THF, using the CPCM model. In studied dye units, the DOS was interpreted by the colors green, blue, and red, where blue color depicts the TDOS, green color depicts the occupied orbitals, and red color depicts the virtual orbitals. The left side of the broken vertical line is the HOMO or valence band, designated by green color, the right side of it is the LUMO or CB, designated by red, and the difference between the two is the band gap. Therefore, the TDOS exhibited by the blue color line increases upon changing the spacer and also upon increasing the number of spacer units. From the DOS graph (Figure 4), the double identical π-spacer unit (DA2, DA5, and DA6) showed a better overlapping density of the states than the single attached spacer unit molecules (DA1, DA3, and DA4), thereby supporting the frontier molecular orbital (FMO) contribution. In the subsequent studies, we calculated the HOMO−LUMO gap of dye−$(TiO_2)_9$, as reported in Table 1. In comparison to that in isolated dye sensitizers, the energy gaps in dye−$(TiO_2)_9$ systems were found to be lower. The LUMO energy levels are lower than that of the isolated dye molecules, which causes the energy gaps to narrow. Further, we studied the interaction of the dye−$(TiO_2)_9$ system with MO@G as a multi-junction system, and the effect of this contact on the energy levels was investigated.

The energy gaps between the HOMO and LUMO were found to be lowered further, indicating improved charge transport and energy conversion efficiency. For the achievement of high performance, graphene-based nanocomposites play a vital role due to their excellent compatibility with different active components (metal oxides).[72] The charge transfer efficiency of graphene-based materials will be much improved if they are decorated and suppress the aggregation as well, which will result in an enhancement of the electrochemical stability.[73]

5. ABSORPTION STUDIES

5.1. D−π−A Absorption Systems. The UV−visible absorption spectroscopy was carried out by using the B3LYP/6-311G(d,p) level of theory, and the optimized geometries of DA1−DA6 are shown in Figure 5. The

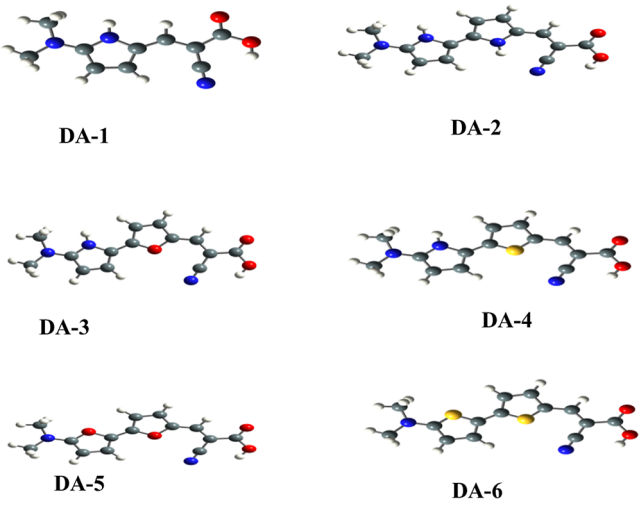

Figure 5. Optimized Geometries of DA1−DA6 optimized using the B3LYP-(6-311G(d,p)) level of theory.

absorption spectra of dye-sensitizer molecules were found to have two absorption bands with wavelengths ranging from 300 to 450 and 450 to 800 nm. The lower wavelength absorptions are due to the π−π* transitions within the organic scaffold, whereas the higher wavelength absorptions correspond to the intramolecular charge transfer (ICT) from the donor to the acceptor via the π-bridge. The maximum absorption wavelength λ_{max} for the systems were found to be 403.06, 527.04, 528.34, 571.34, 581.54, and 538.27 nm for DA1, DA2, DA3, DA4, DA5, and DA6, respectively (Figure 7A).

All the studied systems (DA2−DA6) show a bathochromic shift concerning the parent molecule DA1. Thus, the DA2−DA6 is expected to harvest light in a long wavelength region and so have some advantage over the parent dye molecule. Furthermore, we found that the HOMO to LUMO excitations for DA1, DA2, DA3, DA4, DA5, and DA6 contribute mostly to the charge transfer band. These excitations are due to the ICT from the donor to the cyano-acrylic acid acceptor part of the molecule. Table2 lists the dye sensitizers' excited singlet states, transition energies, oscillator strengths, and λ_{max}. As such, we can safely ascribe the higher wavelength absorption and thus increased LHE to ICT.

https://doi.org/10.1021/acsomega.3c00333
ACS Omega 2023, 8, 8865−8875

Table 2. FMOs of GO and Sb_2O_3@GO

mol	E_{HOMO} (eV)	E_{LUMO} (eV)	HOMO−LUMO gap (eV)
GO	−6.19	−2.85	3.34
Sb_2O_3@GO	−7.1	−5.687	1.42

5.2. Dye−$(TiO_2)_9$ Absorption Systems. The UV−visible absorbance of the dye−TiO_2 adsorption systems was also studied in the same solvent, and the optimized geometries of dye−TiO_2 are shown in Figure 6. After adsorption,

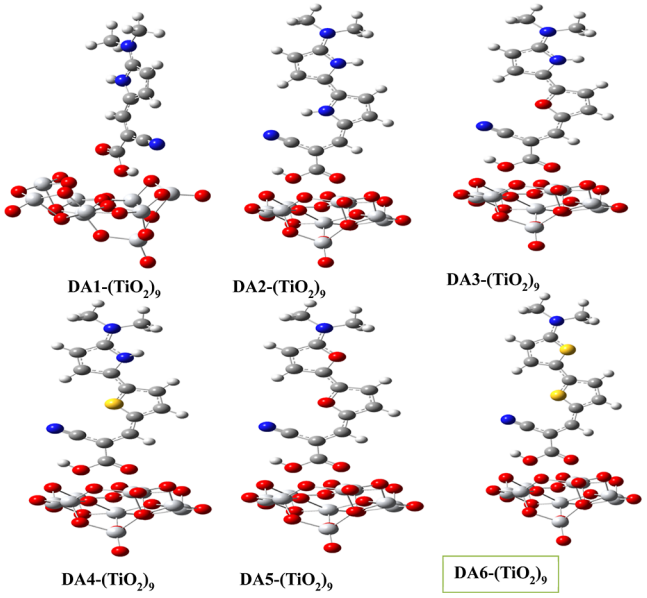

Figure 6. Optimized geometries of the dye−$(TiO_2)_9$ adsorbed systems.

considerable bathochromic shifts were observed in the absorption peaks (Table 2). The spectra primarily correspond to HOMO to LUMO transitions. For DA1−$(TiO_2)_9$, DA2−$(TiO_2)_9$, DA3−$(TiO_2)_9$, DA4−$(TiO_2)_9$, DA5−$(TiO_2)_9$, and DA6−$(TiO_2)_9$, the maximum values for the dye−TiO_2 absorption wavelengths (λ_{max}) are 704.99, 796.55, 807.33, 825.7, 822.99, and 838.56 nm, respectively. In comparison to that of the D−π−A adsorbed systems, the shifts in the absorption peaks are about 301, 269, 279, 254, 241, and 300 nm, respectively (Figure 7B). The shifts suggested that the dye molecules loaded on the $(TiO_2)_9$ semiconductor are affecting the electronic structure and, therefore, the absorption characteristics of the system. Also, in comparison to that of isolated dye molecules, the LUMO orbital energies are seen to shift toward lower energy. The interaction of the dye sensitizer with the positive titanium ions and the electron transfer from the excited state of the dye into the TiO_2 CB stabilizes the LUMO. These findings depict that some charge transfer occurs between the dyes and the semiconductor. As a result, these dyes are expected to act as possible TiO_2 semiconductor sensitizers.

5.3. Dye−TiO_2−MO@G Multi-Junction Systems. *5.3.1. Decoration of Metal Oxide with Graphene.* The graphene-based metal oxide nanocomposites have numerous uses in energy storage and conversion technology, including solar cells, lithium-ion batteries, and supercapacitors.[74] The electrical and optoelectronic characteristics of Sb_2O_3@graphene nanocomposites are significant and helpful enough to be thoroughly investigated by theoretical research. Determination of the proper electronic responses at the atomic scale being challenging, the main factor affecting the optoelectronic and electrical properties of Sb_2O_3@graphene on co-sensitization with a dye sensitizer is yet unknown. Fortunately, a proper insight into the underlying relationship between the interface structure and the optoelectronic properties of Sb_2O_3@graphene on co-sensitization with a D−π_1−π_2−A−TiO_2 sensitizer can be obtained by DFT calculations. The optimization of graphene oxide (GO), Sb_2O_3, and Sb_2O_3@graphene were carried out at the same level of theory as that reported earlier. The anchoring of Sb_2O_3 on the surface of GO takes place through the interaction of the three main functional groups, epoxy, carboxylic acid, and hydroxyl groups on the surface of GO.[75]

The degree of oxidation of GO depends on the source of the graphite, the technique of manufacture, and the length of the synthesis process. Recently, the atomic and electronic structures of GO decorated with various metals have been studied using DFT computations.[58] Gaussian 09 was used to determine the HOMO−LUMO energies of GO and Sb_2O_3@GO. The associated FMO graphs are shown in Figure 3.

It is pertinent to mention that the degree of oxidation of GO depends on the source of the graphite, the technique of manufacture, and the length of the synthesis process. Recently, the atomic and electronic structures of GO decorated with various metals have been studied using DFT computations.[76] Figure 8 shows the optimized structures of GO and metal-oxide-decorated graphene. The interaction energy studies revealed that GO and Sb_2O_3 exhibit an interaction energy value of −236.57 kJ/mol, hence depicting the spontaneity of such an interaction. Moreover, FMO analysis was carried out for the Sb_2O_3@GO system. The FMO plots (Figure 9) show that Sb_2O_3@GO has a small energy gap when compared to GO. Sb_2O_3@GO was found to have an energy gap of 1.42 eV with the HOMO of value −7.1 eV and the LUMO of value −5.687 eV (Table 2), whereas the energy gap of GO was 3.34 eV with the HOMO of value −6.19 eV and the LUMO of value −2.85 eV, which also depend upon the experiments.[77] The GO band gap decreased when decorated with Sb_2O_3, improving its charge transport properties.

5.3.2. Dye−$(TiO_2)_9$/Sb_2O_3@GO Absorption Systems. Solar cells having numerous p−n junctions composed of various semiconductor materials are known as multi-junction solar cells. Various light wavelengths will cause the p−n junction of each material to generate an electric current. The efficiency of the cells' conversion of solar energy to electrical energy is increased by the employment of several semiconducting materials, which enable the absorbance of a wider spectrum of wavelengths. The multi-junction systems in solar cell technology are considered promising approaches for enhancing light gathering efficiency and overall light conversion efficiency. The optimized geometries of dye−$(TiO_2)_9$/Sb_2O_3@GO depicting the interaction of the D−π_1−π_2−A−TiO_2 system with the Sb_2O_3@GO framework, as a model multi-junction system, are shown in Figure 10, and the effect of this interaction on the system's absorption behavior is given in the Supporting Information (S1). In comparison to that of the dye−TiO_2 adsorbed systems, the absorption peaks of multi-junction systems were found to be further red-shifted (Figure 7C). It means that there is an interaction between dye−TiO_2 and MO@GO. For DA1−$(TiO_2)_9$−MO@GO, DA2−$(TiO_2)_9$−MO@GO, DA3−$(TiO_2)_9$−MO@GO, DA4−

https://doi.org/10.1021/acsomega.3c00333
ACS Omega 2023, 8, 8865−8875

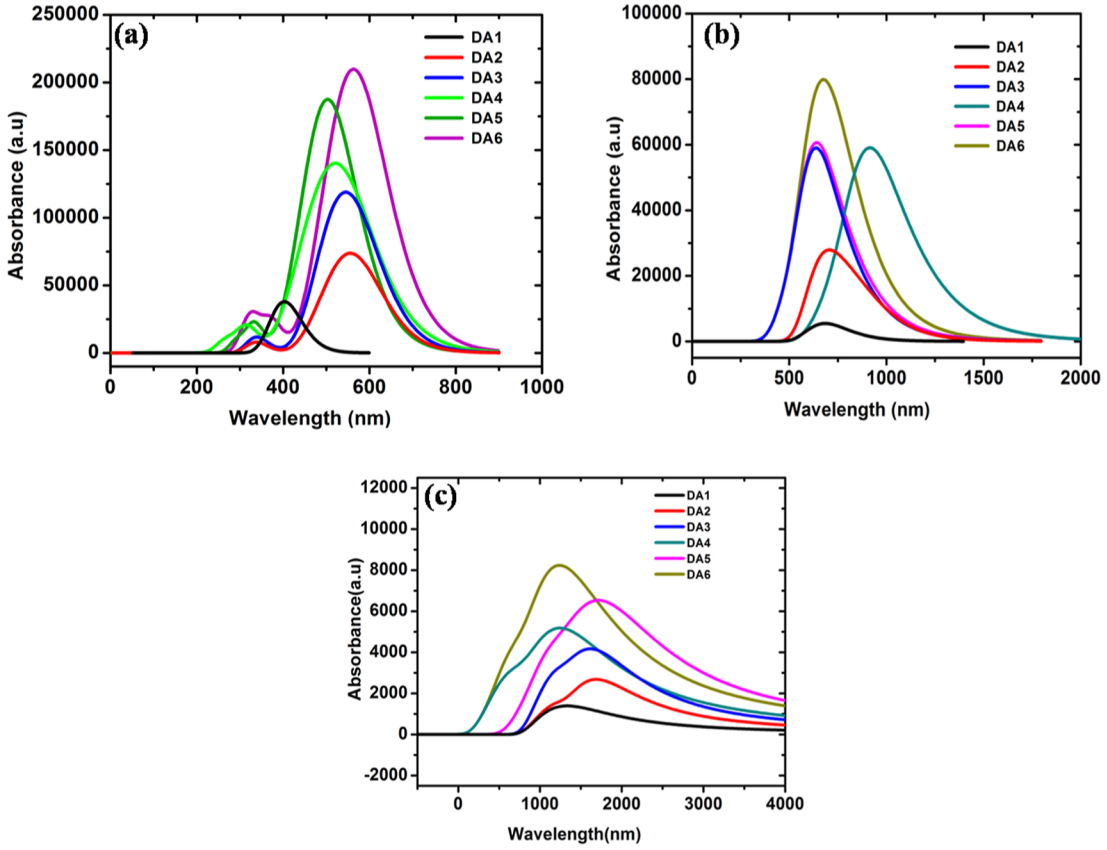

Figure 7. Absorption spectra of (A) (D−π−A of DA1−DA6), (B) (D−π−A/TiO_2 of DA1−DA6), and (C) (D−π−A−TiO_2/MO@G of DA1−DA6).

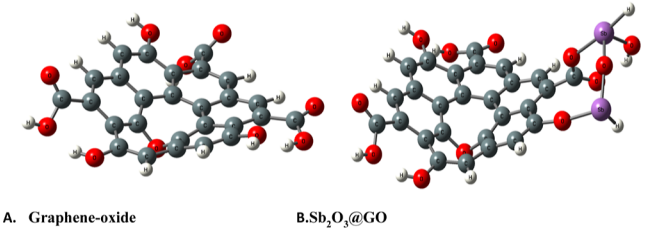

Figure 8. Optimized structures of (A) GO and (B) Sb_2O_3@GO.

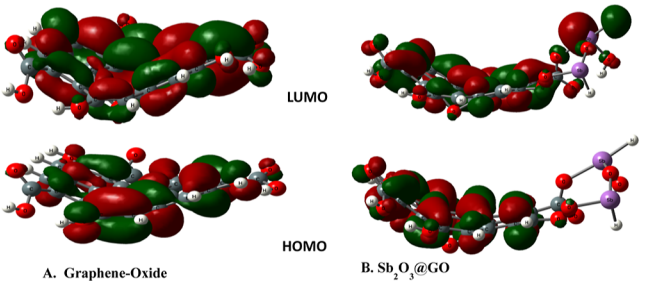

Figure 9. FMOs of (A) GO and (B) Sb_2O_3@GO.

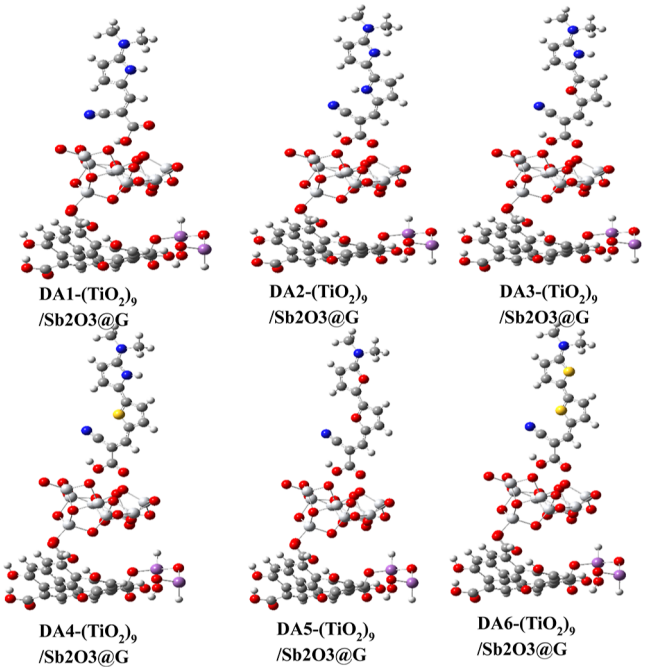

Figure 10. Optimized geometries of the dye−$(TiO_2)_9$/Sb_2O_3@G multi-junction systems adsorbed systems.

$(TiO_2)_9$−MO@GO, DA5−$(TiO_2)_9$−MO@GO, and DA6−$(TiO_2)_9$−MO@GO, the λ_{max} values for these dye−$(TiO_2)_9$−MO@GO multi-junction systems are 1639.3, 1620.51, 1628.23, 1636.92, 1643.29, and 1652.8 nm, respectively. In comparison to that of dye−TiO_2 adsorbed systems, the corresponding changes in maximum absorption wavelengths are about 935, 824, 821, 811, 821, and 814 nm. As a result of its interaction with the MO@GO unit, the dye−TiO_2 system's absorbance behavior has been improved.

https://doi.org/10.1021/acsomega.3c00333
ACS Omega 2023, 8, 8865−8875

Table 3. Photovoltaic Parameters of DA1−DA6 Systems

mol	V_{oc} (eV)	Λ_{max} (nm)	f	LHE	ΔG_{inj} (eV)	μ_{NORMAL}	E^*_{dye} (eV)	ΔG_{reg} (eV)	ΔG_{reorg} (eV)	H−L contribution
DA1	1.72	403.06	0.94	0.88	−1.186	24.96	−2.81	1.09	1.36	H−L = (100%)
DA2	1.55	527.04	1.04	0.91	−1.42	36.19	−2.59	0.13	1.197	H−L = (99%)
DA3	1.25	528.34	1.17	0.93	−1.197	37.99	−2.80	0.35	0.87	H−L = (100%)
DA4	1.41	571.34	0.77	0.83	−1.29	34.44	−2.71	0.08	0.82	H−L = (99%)
DA5	1.08	518.54	1.22	0.94	−1.00	18.68	−3.00	0.58	−2.449	H−L = (99%)
DA6	1.32	538.27	0.59	0.74	−1.09	13.77	−2.91	0.41	0.82	H−L = (98%)

6. PHOTOVOLTAIC PARAMETERS

For the development of efficient DSSCs, improved photovoltaic parameters including LHE, excited-state oxidation potential (E^*_{dye}), the free energy of electron injection (G_{inject}), electron injection efficiency (inject), total reorganization energy (λ_{total}), and open voltage (V_{oc}) are essential. The results of the calculations are tabulated (Table2). The absorptivity of a sensitizer, and, hence, its ability to harness available solar radiations, is reflected in its LHE. A sensitizer should have a good LHE value for effective sensitization; the higher the LHE value is, the more efficient the sensitizer is. The LHE values for all the dye molecules under consideration (DA1−DA6) were evaluated and were found to exhibit the following trend: DA5 > DA3 > DA2 > DA1 > DA4 > DA6. The results reflect that all the sensitizers show good values of LHE, with DA5 and DA3 showing better values of LHE and hence being expected to be good sensitizers. All dyes' HOMO and LUMO orbital densities (the gross orbital population of the Mulliken charge) were analyzed using the Gauss Sum program, and the contributions from each moiety are listed in Table 3. The D−A moiety is dispersed by the orbital densities of the HOMO to LUMO, which are 100, 99, 100, 99, 99, and 98% forDA1, DA2, DA3, DA4, DA5, and DA6, respectively. These numbers demonstrate that the HOMO and LUMO distributions of the dyes are distinct, indicating that the HOMO LUMO transition can be viewed as an ICT, one of the key properties of D−A-based dyes. The desired effective electron transfer with considerable light absorption is also made possible by this feature.

Furthermore, the free energy of electron injection (ΔG_{inject}) must be advantageous for fast and effective electron transfer from the excited state of a dye sensitizer to the semiconductor CB. The value of G_{inject} indicates how easily electrons can be injected from the sensitizer (through its acceptor group) into the semiconductor CB and hence the DSSC's efficiency. The ΔG_{inject} values for the dye molecules were evaluated and show the following trend: DA2 > DA4 > DA3 > DA1 > DA6 > DA5. Sensitizers will inject electrons in the reverse sequence. All of the dye sensitizers had adequate electron injection efficiencies, with DA5 and DA6 having the best electron injection efficiencies. The reorganization parameter (ΔG_{reorg}) is used to evaluate the geometry relaxations that occur during electron injection and dye regeneration. Lower reorganization energy levels are essential for a successful electron transfer process. For each sensitizer, we calculated the overall reorganization energy. According to Marcus' model, lower reorganization values indicate effective electron transmission across the intramolecular interface. The calculated values of reorganization energies for the dye molecules (DA1−DA6) show the following order: DA5 < DA6 ∼ DA4 < DA3 < DA2 < DA1. As a result, the dye sensitizer's ease of electron transfer will follow the reverse order. Furthermore, among the sensitizers under investigation, DA5 has the lowest total reorganization energy and is thus projected to be a better sensitizer. Apart from the efficiency parameters already given, the open-circuit voltage (V_{oc}) is also worth mentioning. It is the voltage achieved in a DSSC under zero dark current conditions, i.e. when no inhibitive processes such as back electron recombination processes are operative. The open-circuit voltage must be higher for a more efficient sensitizer and, as a result, a more efficient DSSC. A DSSC's efficiency can be improved by any strategy that inhibits recombination activities. The V_{oc} values for the sensitizers were calculated, and based on the computed results, sensitizer DA5 shows the least value of total reorganization energies and the least time to inject an electron into the CB of TiO_2 and has a higher LHE, which also suggests that DA5 allows a much easier charge transport across the semiconductor interface and is therefore expected to be beneficial for designing efficient DSSCs.

7. INTERACTION ENERGIES OF DYE−$(TIO_2)_9$ AND DYE−$(TIO_2)_9$/MO@G MULTI-JUNCTION SYSTEMS

The interaction energy studies were carried out for dye−$(TiO_2)_9$ and dye−$(TiO_2)_9$/MO@G multi-junction systems. The interaction energy was calculated by the following relations

$$\text{interaction energy} = E_{COMPLEX} - [(E_A) + (E_B)] \quad (9)$$

Here, from eq 9, the complex is Dye−$(TiO_2)_9$, A is the dye, and B is TiO_2

$$\text{interaction energy} = E_{COMPLEX} - [(E_A) + (E_B)] \quad (10)$$

Here, from eq 10, the complex is dye−$(TiO_2)_9$/MO@G multi-junction systems, A is dye−$(TiO_2)_9$, and B is MO@G. The values of the interaction of (eqs 9 and 10) are shown in (Table 4).

Table 4. Interaction Energy Values (kJ/mol) of the Various Dye−$(TiO_2)_9$ and Dye−$(TiO_2)_9$/MO@G Multi-Junction Systems

dye	dye−$(TiO_2)_9$	dye−$(TiO_2)_9$/MO@G
DA1	−63.012	−283.55
DA2	−199.53	−420.08
DA3	−173.28	−446.335
DA4	−223.16	−656.375
DA5	−170.65	−354.44
DA6	−210.04	−680.004

The interaction energy shows the following order of DA4−TiO_2 < DA6−TiO_2 < DA2−TiO_2 < DA3−TiO_2 < DA5−TiO_2 < DA1−TiO_2 for dye−TiO_2 adsorbed systems and DA6−TiO_2/MO@G < DA4−TiO_2/MO@G < DA3−TiO_2/MO@GO < DA2−TiO_2/MO@GO < DA5−TiO_2/MO@GO < DA1−TiO_2/MO@GO for dye−TiO_2/MO@GO multi-junction systems.

https://doi.org/10.1021/acsomega.3c00333
ACS Omega 2023, 8, 8865−8875

The results show that all the adsorbed systems exhibit a favorable value of interaction energy, leading to a beneficial interaction. The interaction of the dye with TiO_2 is favorable, as can be seen from the red shifts in the case of UV spectra (Figure 7B). Also, the interaction of the MO@G framework with the dye−TiO_2 adsorbed systems and the consequent red shifts in the maximum absorption wavelengths can be linked to the interaction, which we can easily visualize from Figure 7C. The study reveals that the interaction increases when the dye−TiO_2 systems are adsorbed on the MO@G framework, leading to the formation of multi-junction systems. Therefore, these multi-junction systems are supposed to improve the PCE of the future solar energy devices.

8. CONCLUSIONS

In this work, a series of D−π−A systems and D−π_1−π_2−A systems were investigated to provide comprehensive information about the optical, optoelectronic, and photovoltaic properties of the DA1−DA6 dye-based light-harvesting systems using DFT and TD-DFT. Various spacer units were used to show better optoelectronic properties. The FMO studies revealed that the LUMO of all the systems based on DA1−DA6 lies above the CB of TiO_2, whereas their HOMO lies below the HOMO of the redox mediator for a better electron injection process and dye regeneration. From the absorption spectra and several other parameters, the DA5 system is expected to exhibit a better performance in the DSSC. The dye−$(TiO_2)_9$/Sb_2O_3@GO multi-junction systems proves to be a more effective light-harvesting unit, with better photovoltaic, optoelectronic, and charge transport properties than that of the D−π_1−π_2−A dye/TiO_2 system. The improved interaction between the dye−TiO_2 adsorbed systems with MO@G is also supported by better interaction energy values. This theoretical work indicates that the multi-junction systems based on metal oxide-decorated graphene−D−π_1−π_2−A dye-sensitized TiO_2 nanocomposites may open promising opportunities for the fabrication of commercially viable DSSCs with improved absorption efficiencies in a wide range of the solar spectrum.

■ ASSOCIATED CONTENT

Supporting Information

The Supporting Information is available free of charge at https://pubs.acs.org/doi/10.1021/acsomega.3c00333.

Interaction energy; charge density and interaction energy of MO@GO; and Cartesian coordinates of the DFT optimized geometry for DA1−DA6 (PDF)

■ AUTHOR INFORMATION

Corresponding Author

Altaf Hussain Pandith − *Laboratory of Nanoscience and Quantum Computations, Department of Chemistry, University of Kashmir, Srinagar 190006 J&K, India;* orcid.org/0000-0002-2601-5580; Phone: +91-194-2424900, +91-7006429021; Email: altafpandit23@gmail.com; Fax: +91-194-2414049

Authors

Kaniz Fatima − *Laboratory of Nanoscience and Quantum Computations, Department of Chemistry, University of Kashmir, Srinagar 190006 J&K, India*

Taniya Manzoor − *Laboratory of Nanoscience and Quantum Computations, Department of Chemistry, University of Kashmir, Srinagar 190006 J&K, India*

Aaliya Qureashi − *Laboratory of Nanoscience and Quantum Computations, Department of Chemistry, University of Kashmir, Srinagar 190006 J&K, India*

Complete contact information is available at: https://pubs.acs.org/10.1021/acsomega.3c00333

Notes

The authors declare no competing financial interest.

■ ACKNOWLEDGMENTS

We acknowledge the Department of Science and Technology, Government of India, New Delhi, for providing facilities under the DST-PURSE Programme (TPN-56945) to the Department of Chemistry, University of Kashmir. We are also thankful to CSIR UGC for providing a fellowship in the form of NET/JRF (F. no. 16.9 (June 2018)/2019).

■ REFERENCES

(1) Hanif, I. Impact of Fossil Fuels Energy Consumption, Energy Policies, and Urban Sprawl on Carbon Emissions in East Asia and the Pacific: A Panel Investigation. *Energy Strategy Rev.* **2018**, *21*, 16−24.

(2) Perera, F.; Ashrafi, A.; Kinney, P.; Mills, D. Towards a fuller assessment of benefits to children's health of reducing air pollution and mitigating climate change due to fossil fuel combustion. *Environ. Res.* **2019**, *172*, 55−72.

(3) Perera, F. P. Multiple Threats to Child Health from Fossil Fuel Combustion: Impacts of Air Pollution and Climate Change. *Environ. Health Prospects* **2017**, *125*, 141−148.

(4) Jha, S. K.; Bilalovic, J.; Jha, A.; Patel, N.; Zhang, H. Renewable energy: Present research and future scope of Artificial Intelligence. *Renewable Sustainable Energy Rev.* **2017**, *77*, 297−317.

(5) Benedek, J.; Sebestyén, T. T.; Bartók, B. Evaluation of Renewable Energy Sources in Peripheral Areas and Renewable Energy-Based Rural Development. *Renewable Sustainable Energy Rev.* **2018**, *90*, 516−535.

(6) Sarmah, A.; Hobza, P. Directly Linked Metalloporphyrins: A Quest for Bio-Inspired Materials. *Mater. Adv.* **2020**, *1*, 1895−1908.

(7) Qazi, A.; Hussain, F.; Rahim, N. A. B. D.; Hardaker, G.; Alghazzawi, D.; Shaban, K.; Haruna, K. Towards Sustainable Energy: A Systematic Review of Renewable Energy Sources, Technologies, and Public Opinions. *IEEE Access* **2019**, *7*, 63837−63851.

(8) O'Regan, B.; Grätzel, M. A low-cost, high-efficiency solar cell based on dye-sensitized colloidal TiO_2 films. *Nature* **1991**, *353*, 737−740.

(9) Jadhav, M.; Vaghasiya, J. V.; Patil, D.; Soni, S. S.; Sekar, N. Effect of donor modification on the photo-physical and photo-voltaic properties of N-alkyl/aryl amine based chromophores. *New J. Chem.* **2019**, *43*, 8970−8981.

(10) Tercan, M.; Dayan, O. Synthesis and DSSC Applications of Ru(II) Complexes Bearing Benzimidazole Type Ligands. *J. Electron. Mater.* **2019**, *48*, 642−648.

(11) El Mzioui, S.; Bouzzine, S. M.; Sidir, İ.; Bouachrine, M.; Bennani, M. N.; Bourass, M.; Hamidi, M. Theoretical investigation on π-spacer effect of the D-π-A organic dyes for dye-sensitized solar cell applications: a DFT and TD-BHandH study. *J. Solid State Chem.* **2019**, *25*, 92.

(12) Qin, C.; Numata, Y.; Zhang, S.; Islam, A.; Yang, X.; Sodeyama, K.; Tateyama, Y.; Han, L. A Near-Infraredcis-Configured Squaraine Co-Sensitizer for High-Efficiency Dye-Sensitized Solar Cells. *J. Mol. Graphics Modell.* **2013**, *23*, 3782−3789.

(13) Chang, D. W.; Lee, H. J.; Kim, J. H.; Park, S. Y.; Park, S.-M.; Dai, L.; Baek, J.-B. Novel Quinoxaline-Based Organic Sensitizers for Dye-Sensitized Solar Cells. *Org. Lett.* **2011**, *13*, 3880−3883.

(14) Saranya, K.; Rameez, M.; Subramania, A. Developments in Conducting Polymer Based Counter Electrodes for Dye-Sensitized Solar Cells - An Overview. *Eur. Polym. J.* **2015**, *66*, 207−227.
(15) Krishna, N. V.; Krishna, J. S. V.; Singh, S. P.; Han, L.; Giribabu, L.; Bedja, I. M.; Gupta, R. K.; Islam, A. Donor-π-Acceptor Based Stable Porphyrin Sensitizers for Dye-Sensitized Solar Cells: Effect of π-Conjugated Spacers. *J. Phys. Chem. C* **2017**, *121*, 6464.
(16) Shi, X.; Li, Y.; Wang, L. Two Novel Mono-Hydroxyl Pyranoanthocyanidins Bearing Dimethylamino Substituent(s) for Dye-Sensitized Solar Cell. *J. Mol. Struct.* **2022**, *1252*, 132055.
(17) Parwaiz, S.; Bhunia, K.; Das, A. K.; Khan, M. M.; Pradhan, D. Cobalt-Doped Ceria/Reduced Graphene Oxide Nanocomposite as an Efficient Oxygen Reduction Reaction Catalyst and Supercapacitor Material. *J. Phys. Chem. C* **2017**, *121*, 20165−20176.
(18) Allen, M. J.; Tung, V. C.; Kaner, R. B. Honeycomb Carbon: A Review of Graphene. *Chem. Rev.* **2010**, *110*, 132−145.
(19) Raccichini, R.; Varzi, A.; Passerini, S.; Scrosati, B. The Role of Graphene for Electrochemical Energy Storage. *Nat. Mater.* **2015**, *14*, 271−279.
(20) Ortiz Balbuena, J.; Tutor de Ureta, P.; Rivera Ruiz, E.; Mellor Pita, S. Enfermedad de Vogt-Koyanagi-Harada. *Med. Clin.* **2016**, *146*, 93−94.
(21) Chien, C. T.; Li, S. S.; Lai, W. J.; Yeh, Y. C.; Chen, H. A.; Chen, I. S.; Chen, L. C.; Chen, K. H.; Nemoto, T.; Isoda, S.; Chen, M.; Fujita, T.; Eda, G.; Yamaguchi, H.; Chhowalla, M.; Chen, C. W. Tunable Photoluminescence from Graphene Oxide. *Angew. Chem., Int. Ed.* **2012**, *51*, 6662−6666.
(22) Chen, H.; Wei, Q.; Saidaminov, M. I.; Wang, F.; Johnston, A.; Hou, Y.; Peng, Z.; Xu, K.; Zhou, W.; Liu, Z.; Qiao, L.; Wang, X.; Xu, S.; Li, J.; Long, R.; Ke, Y.; Sargent, E. H.; Ning, Z. Efficient and Stable Inverted Perovskite Solar Cells Incorporating Secondary Amines. *Adv. Mater.* **2019**, *31*, 1903559.
(23) Ye, C.; Wang, G.; Kong, M.; Zhang, L. Controlled Synthesis ofSb2O3Nanoparticles, Nanowires, and Nanoribbons. *J. Nanomater.* **2006**, *2006*, 1−5.
(24) Ge, S.; Wang, Q.; Li, J.; Shao, Q.; Wang, X. Controllable Synthesis and Formation Mechanism of Bow-Tie-like Sb2O3 Nanostructures via a Surfactant-Free Solvothermal Route. *J. Alloys Compd.* **2010**, *494*, 169−174.
(25) Guo, L.; Wu, Z.; Liu, T.; Wang, W.; Zhu, H. Synthesis of Novel Sb2O3 and Sb2O5 Nanorods. *Chem. Phys. Lett.* **2000**, *318*, 49−52.
(26) Deng, Z.; Chen, D.; Tang, F.; Ren, J.; Muscat, A. J. Synthesis and Purple-Blue Emission of Antimony Trioxide Single-Crystalline Nanobelts with Elliptical Cross Section. *Nano Res.* **2009**, *2*, 151−160.
(27) Kaviyarasu, K.; Sajan, D.; Devarajan, P. A. A Rapid and Versatile Method for Solvothermal Synthesis of Sb2O3 Nanocrystals under Mild Conditions. *Appl. Nanosci.* **2013**, *3*, 529−533.
(28) Tigau, N.; Ciupina, V.; Prodan, G. The Effect of Substrate Temperature on the Optical Properties of Polycrystalline Sb2O3 Thin Films. *J. Cryst. Growth* **2005**, *277*, 529−535.
(29) Sahoo, N. K.; Apparao, K. V. S. R. Process-Parameter Optimization of Sb2O3 Films in the Ultraviolet and Visible Region for Interferometric Applications. *Appl. Phys. A: Mater. Sci. Process.* **1996**, *63*, 195−202.
(30) Chang, H.; Wu, H. Graphene-Based Nanocomposites: Preparation, Functionalization, and Energy and Environmental Applications. *Energy Environ. Sci.* **2013**, *6*, 3483−3507.
(31) Khan, M.; Tahir, M. N.; Adil, S. F.; Khan, H. U.; Siddiqui, M. R. H.; Al-warthan, A. A.; Tremel, W. Graphene Based Metal and Metal Oxide Nanocomposites: Synthesis, Properties and Their Applications. *J. Mater. Chem. A* **2015**, *3*, 18753−18808.
(32) Sánchez-de-Armas, R.; Oviedo López, J.; San-Miguel, M. A.; Sanz, J. F.; Ordejón, P.; Pruneda, M. Real-Time TD-DFT Simulations in Dye Sensitized Solar Cells: The Electronic Absorption Spectrum of Alizarin Supported on TiO2 Nanoclusters. *J. Chem. Theory Comput.* **2010**, *6*, 2856−2865.
(33) Sánchez-de-Armas, R.; San Miguel, M. Á.; Oviedo, J.; Sanz, J. F. Coumarin Derivatives for Dye Sensitized Solar Cells: A TD-DFT Study. *Phys. Chem. Chem. Phys.* **2012**, *14*, 225−233.
(34) Narayan, M. R. Review: Dye Sensitized Solar Cells Based on Natural Photosensitizers. *Renewable Sustainable Energy Rev.* **2011**, *16*, 208−215.
(35) Usami, A.; Seki, S.; Mita, Y.; Kobayashi, H.; Miyashiro, H.; Terada, N. Temperature Dependence of Open-Circuit Voltage in Dye-Sensitized Solar Cells. *Sol. Energy Mater. Sol. Cells* **2009**, *93*, 840−842.
(36) Zhang, Z. L.; Zou, L. Y.; Ren, A. M.; Liu, Y. F.; Feng, J. K.; Sun, C. C. Theoretical Studies on the Electronic Structures and Optical Properties of Star-Shaped Triazatruxene/Heterofluorene Co-Polymers. *Dyes Pigm.* **2013**, *96*, 349−363.
(37) Biswas, A. K.; Barik, S.; Sen, A.; Das, A.; Ganguly, B. Design of Efficient Metal-Free Organic Dyes Having an Azacyclazine Scaffold as the Donor Fragment for Dye-Sensitized Solar Cells. *J. Phys. Chem. C* **2014**, *118*, 20763−20771.
(38) Preat, J.; Jacquemin, D.; Michaux, C.; Perpète, E. A. Improvement of the Efficiency of Thiophene-Bridged Compounds for Dye-Sensitized Solar Cells. *Chem. Phys.* **2010**, *376*, 56−68.
(39) De Angelis, F.; Fantacci, S.; Selloni, A. Alignment of the dye's molecular levels with the TiO2band edges in dye-sensitized solar cells: a DFT-TDDFT study. *Nanotechnology* **2008**, *19*, 424002.
(40) Odobel, F.; Le Pleux, L.; Pellegrin, Y.; Blart, E. New Photovoltaic Devices Based on the Sensitization of P-Type Semiconductors: Challenges and Opportunities. *Acc. Chem. Res.* **2010**, *43*, 1063−1071.
(41) Marcus, R. A. On the Theory of Oxidation-Reduction Reactions Involving Electron Transfer. III. Applications to Data on the Rates of Organic Redox Reactions. *J. Chem. Phys.* **1957**, *26*, 872−877.
(42) Balanay, M. P.; Kim, D. H. Structures and Excitation Energies of Zn-Tetraarylporphyrin Analogues: A Theoretical Study. *J. Mol. Struct.: THEOCHEM* **2009**, *910*, 20−26.
(43) Frisch, M. J.; Trucks, G. W.; Schlegel, H. B.; Scuseria, G. E.; Robb, M. A.; Cheeseman, J. R.; Scalmani, G.; Barone, V.; Petersson, G. A.; Nakatsuji, H.; Li, X.; Caricato, M.; Marenich, A.; Bloino, J.; Janesko, B. G.; Gomperts, R.; Mennucci, B.; Hratchian, H. P.; Ortiz, J. V.; Izmaylov, A. F.; Sonnenberg, J. L.; Williams-Young, D.; Ding, F.; Lipparini, F.; Egidi, F.; Goings, J.; Peng, B.; Petrone, A.; Henderson, T.; Ranasinghe, D.; Zakrzewski, V. G.; Gao, J.; Rega, N.; Zheng, G.; Liang, W.; Hada, M.; Ehara, M.; Toyota, K.; Fukuda, R.; Hasegawa, J.; Ishida, M.; Nakajima, T.; Honda, Y.; Kitao, O.; Nakai, H.; Vreven, T.; Throssell, K.; Montgomery, J. A., Jr.; Peralta, J. E.; Ogliaro, F.; Bearpark, M.; Heyd, J. J.; Brothers, E.; Kudin, K. N.; Staroverov, V. N.; Keith, T.; Kobayashi, R.; Normand, J.; Raghavachari, K.; Rendell, A.; Burant, J. C.; Iyengar, S. S.; Tomasi, J.; Cossi, M.; Millam, J. M.; Klene, M.; Adamo, C.; Cammi, R.; Ochterski, J. W.; Martin, R. L.; Morokuma, K.; Farkas, O.; Foresman, J. B.; Fox, D. J. *Gaussian 09*, Revision A.02; Gaussian, Inc.: Wallingford CT, 2016.
(44) Becke, A. D. Density-Functional Thermochemistry. V. Systematic Optimization of Exchange-Correlation Functionals. *J. Chem. Phys.* **1997**, *107*. 8554.DOI: DOI: 10.1063/1.475007.
(45) Abbas, G.; Irfan, A.; Mir, M.; Mariya-al-Rashida; Khan, A. F. Electronic Structure and Absorption Spectra of 6-Picoline Schiff Base: A DFT and XRD Based Approach. *J. Mol. Struct.* **2013**, *1050*, 10−14.
(46) Becke, A. D. Density-functional thermochemistry. III. The role of exact exchange. *J. Chem. Phys.* **1993**, *98*, 5648−5652.
(47) Stephens, P. J.; Devlin, F. J.; Chabalowski, C. F.; Frisch, M. J. Ab Initio Calculation of Vibrational Absorption and Circular Dichroism Spectra Using Density Functional Force Fields. *J. Phys. Chem.* **1994**, *98*, 11623−11627.
(48) Perdew, J. P.; Chevary, J. A.; Vosko, S. H.; Jackson, K. A.; Pederson, M. R.; Singh, D. J.; Fiolhais, C. Erratum: Atoms, molecules, solids, and surfaces: Applications of the generalized gradient approximation for exchange and correlation. *Phys. Rev. B: Condens. Matter Mater. Phys.* **1993**, *48*, 4978.
(49) Venkatraman, R.; Panneer, S. V. K.; Varathan, E.; Subramanian, V. Aromaticity-Photovoltaic Property Relationship of Triphenylamine-Based D-π-A Dyes: Leads from DFT Calculations. *J. Phys. Chem. A* **2020**, *124*, 3374−3385.

https://doi.org/10.1021/acsomega.3c00333
ACS Omega 2023, 8, 8865−8875

(50) Yang, Z.; Liu, C.; Shao, C.; Lin, C.; Liu, Y. First-Principles Screening and Design of Novel Triphenylamine-Based D−π-A Organic Dyes for Highly Efficient Dye-Sensitized Solar Cells. *J. Phys. Chem. C* **2015**, *119*, 21852−21859.
(51) Wu, F.; Lee, L. T. L.; Liu, J.; Zhao, S.; Chen, T.; Wang, M.; Zhong, C.; Zhu, L. Novel Organic Dyes Based on Diarylmethylene-Bridged Triphenylamine for Dye-Sensitized Solar Cells. *Synth. Met.* **2015**, *205*, 70−77.
(52) Al-Sehemi, A. G.; Allami, S. A. S.; Kalam, A. Design and Synthesis of Organic Dyes with Various Donor Groups: Promising Dyes for Dye-Sensitized Solar Cells. *Bull. Mater. Sci.* **2020**, *43*, 224.
(53) Cossi, M.; Rega, N.; Scalmani, G.; Barone, V. Energies, Structures, and Electronic Properties of Molecules in Solution with the C-PCM Solvation Model. *J. Comput. Chem.* **2003**, *24*, 669−681.
(54) Leszczynski, J.; Kaczmarek-Kedziera, A.; Puzyn, T.; Papadopoulos, M. G.; Reis, H.; Shukla, M. K. *Handbook of Computational Chemistry*; Springer International Publishing, 2017.
(55) Allouche, A.-R. Gabedit. A Graphical User Interface for Computational Chemistry Softwares. *J. Comput. Chem.* **2012**, *32*, 174−182.
(56) Saha, A.; Ganguly, B. A DFT Study to Probe Homo-Conjugated Norbornylogous Bridged Spacers in Dye-Sensitized Solar Cells: An Approach to Suppressing Agglomeration of Dye Molecules. *RSC Adv.* **2020**, *10*, 15307−15319.
(57) Meti, P.; Nagaraju, G.; Yang, J. W.; Jung, S. H.; Gong, Y. D. Synthesis of dipyrrolopyrazine-based sensitizers with a new π-bridge end-capped donor-acceptor framework for DSSCs: a combined experimental and theoretical investigation. *New J. Chem.* **2019**, *43*, 3017−3025.
(58) Manoharan, S.; Asiri, A. M.; Anandan, S. Impact of anchoring groups for improving the binding nature of organic dyes toward high efficient dye sensitized solar cells. *Sol. Energy* **2016**, *126*, 22−31.
(59) Arslan, B. S.; Güzel, E.; Kaya, T.; Durmaz, V.; Keskin, M.; Avcı, D.; Nebioğlu, M.; Şişman, İ. Novel D-π-A organic dyes for DSSCs based on dibenzo[b,h][1,6]naphthyridine as a π-bridge. *Dyes Pigm.* **2019**, *164*, 188−197.
(60) Subbaiah, M.; Sekar, R.; Palani, E.; Sambandam, A. One-Pot Synthesis of Metal Free Organic Dyes Containing Different Acceptor Moieties for Fabrication of Dye-Sensitized Solar Cells. *Tetrahedron Lett.* **2013**, *54*, 3132−3136.
(61) Calogero, G.; Sinopoli, A.; Citro, I.; Di Marco, G.; Petrov, V.; Diniz, A. M.; Parola, A. J.; Pina, F. Synthetic Analogues of Anthocyanins as Sensitizers for Dye-Sensitized Solar Cells. *Photochem. Photobiol. Sci.* **2013**, *12*, 883−894.
(62) Nicksonsebastin, D.; Pounraj, P.; M, M. *Donor Functionalized Perylene and Different π-Spacers Based Sensitizers for DSSC Applications—A Theoretical Approach*; Research Square, 2021.
(63) Mersal, G. A. M.; Toghan, A.; Yahia, I. S.; El-Sheshtawy, H. S. Pyrrole/thiophene π-bridged two triphenylamine electron donor and substituted thiobarbituric electron acceptor for D-π-A-D- featured DSSC applications. *J. Chin. Chem. Soc.* **2021**, *68*, 1842−1851.
(64) Agneeswari, R.; Kim, D.; Park, S. W.; Jang, S.; Yang, H. S.; Shin, I.; Jeong, J. H.; Tamilavan, V.; Jung, Y. K.; Park, S. H. Influence of thiophene and furan π-bridge on the properties of poly-(benzodithiophene-alt-bis(π-bridge)pyrrolopyrrole-1,3-dione) for organic solar cell applications. *Polymer* **2021**, *229*, 123991.
(65) Agneeswari, R.; Kim, D.; Park, S. W.; Jang, S.; Yang, H. S.; Shin, I.; Jeong, J. H.; Tamilavan, V.; Jung, Y. K.; Park, S. H. Influence of thiophene and furan π-bridge on the properties of poly-(benzodithiophene-alt-bis(π-bridge)pyrrolopyrrole-1,3-dione) for organic solar cell applications. *Polymer* **2021**, *229*, 123991.
(66) Hansen, T. K.; Lakshmikantham, M. V.; Cava, M. P.; Niziurski-Mann, R. E.; Jensen, F.; Becher, J. New extended .pi.-electron donors. Tetrathiafulvalene systems with heterocyclic spacer groups. *J. Am. Chem. Soc.* **1992**, *114*, 5035−5039.
(67) Manzoor, T.; Asmi, S.; Niaz, S.; Pandith, A. H. Computational studies on optoelectronic and charge transfer properties of some perylene-based donor-π-acceptor systems for dye sensitized solar cell applications. *Int. J. Quantum Chem.* **2017**, *117*, No. e25332.
(68) Zhang, L.; Cole, J. M. Anchoring Groups for Dye-Sensitized Solar Cells. *ACS Appl. Mater. Interfaces* **2015**, *7*, 3427−3455.
(69) Zhang, L.; Yang, X.; Li, S.; Yu, Z.; Hagfeldt, A.; Sun, L. Electron-Withdrawing Anchor Group of Sensitizer for Dye-Sensitized Solar Cells, Cyanoacrylic Acid, or Benzoic Acid? *Sol. RRL* **2020**, *4*, 1900436.
(70) Mai, C. L.; Moehl, T.; Hsieh, C. H.; Décoppet, J. D.; Zakeeruddin, S. M.; Grätzel, M.; Yeh, C. Y. Porphyrin Sensitizers Bearing a Pyridine-Type Anchoring Group for Dye-Sensitized Solar Cells. *ACS Appl. Mater. Interfaces* **2015**, *7*, 14975−14982.
(71) Mai, C. L.; Moehl, T.; Hsieh, C. H.; Décoppet, J. D.; Zakeeruddin, S. M.; Grätzel, M.; Yeh, C. Y. Porphyrin Sensitizers Bearing a Pyridine-Type Anchoring Group for Dye-Sensitized Solar Cells. *ACS Appl. Mater. Interfaces* **2015**, *7*, 14975−14982.
(72) Khan, M.; Tahir, M. N.; Adil, S. F.; Khan, H. U.; Siddiqui, M. R. H.; Al-warthan, A. A.; Tremel, W. Graphene Based Metal and Metal Oxide Nanocomposites: Synthesis, Properties and Their Applications. *J. Mater. Chem. A* **2015**, *3*, 18753−18808.
(73) Guo, C. X.; Guai, G. H.; Li, C. M. Graphene Based Materials: Enhancing Solar Energy Harvesting. *Adv. Energy Mater.* **2011**, *1*, 448−452.
(74) Mahmood, N.; Zhang, C.; Yin, H.; Hou, Y. Graphene-Based Nanocomposites for Energy Storage and Conversion in Lithium Batteries, Supercapacitors and Fuel Cells. *J. Mater. Chem. A* **2014**, *2*, 15−32.
(75) Li, Z.; Young, R. J.; Wang, R.; Yang, F.; Hao, L.; Jiao, W.; Liu, W. The Role of Functional Groups on Graphene Oxide in Epoxy Nanocomposites. *Polymer* **2013**, *54*, 5821−5829.
(76) Panigrahi, P.; Dhinakaran, A. K.; Sekar, Y.; Ahuja, R.; Hussain, T. Efficient Adsorption Characteristics of Pristine and Silver-Doped Graphene Oxide Towards Contaminants: A Potential Membrane Material for Water Purification? *ChemPhysChem* **2018**, *19*, 2250−2257.
(77) Kachere, A. R.; Kakade, P. M.; Kanwade, A. R.; Dani, P.; Mandlik, N. T.; Rondiya, S. R.; Dzade, N. Y.; Jadkar, S. R.; Bhosale, S. V. Zinc Oxide/Graphene Oxide Nanocomposites: Synthesis, Characterization and Their Optical Properties. *ES Mater. Manuf.* **2022**, *16*, 19−29.

https://doi.org/10.1021/acsomega.3c00333
ACS Omega 2023, 8, 8865−8875